Astron. Astrophys. 329, 190–198 (1998)

ASTRONOMY AND ASTROPHYSICS

Spectral analyses of WC stars in the LMC⋆

G. Gräfener[1], **W.-R. Hamann**[1], **D.J. Hillier**[2], **and L. Koesterke**[1]

[1] Professur für Astrophysik, Universität Potsdam, Am Neuen Palais 10, D-14469 Potsdam, Germany (goetz@astro.physik.uni-potsdam.de)
[2] Department of Physics and Astronomy, University of Pittsburgh, 3941 O'Hara Street, Pittsburgh, PA 15260, USA

Received 26 June 1997 / Accepted 8 August 1997

Abstract. Spectra of six Wolf-Rayet stars in the Large Magellanic Cloud (LMC) of the subtype WC 4, the dominant WC spectral type in the LMC, are taken with the Faint Object Spectrograph (FOS) on board the Hubble Space Telescope (HST). They are analyzed by means of non-LTE models for spherically expanding atmospheres computed using standard assumptions. Complex model atoms of helium, carbon and oxygen are taken into account.

We find stellar luminosities in the range from $10^{5.1}\,L_\odot$ to $10^{5.6}\,L_\odot$, and mass loss rates of approximately $10^{-4}\ M_\odot\,\mathrm{yr}^{-1}$. The stellar temperature $T_\star$, defined as the effective temperature related to the stellar core radius, is of the order of 100 kK. The atmospheric compositions show carbon mass fractions of about 0.4, oxygen mass fractions in the range 0.1-0.3 and no indications of nitrogen.

Stellar parameters obtained this way build an empirical basis for the understanding of the late evolutionary phases of massive stars. The C/He and O/C abundance ratios are sensitive discriminates of stellar evolutionary models, since they depend, for example, on the adopted mass loss relation, the amount of overshooting, the $^{12}\mathrm{C}\,(\alpha,\gamma)\,^{16}\mathrm{O}$ reaction rate, and the metallicity of the progenitor.

We compare our results to evolutionary calculations and to a galactic sample of WC stars. The deduced abundances agree with some evolutionary calculations, but are in disagreement with others. The derived mass loss rates are found to be in general agreement with common $\dot{M}$-L-relations. Systematic differences between the galactic and the LMC sample exist, possibly reflecting a dependence of WC mass loss on metallicity.

Key words: stars: Wolf-Rayet – stars: abundances – stars: mass loss – Magellanic Clouds

Send offprint requests to: G. Gräfener

⋆ Based on observations a) with the NASA/ESA Hubble Space Telescope, obtained at the Space Telescope Science Institute, which is operated by the Association of Universities for Research in Astronomy, Inc., under NASA contract NAS 5-26555 and b) collected at the European Southern Observatory (ESO), La Silla, Chile.

1. Introduction

Wolf-Rayet (WR) stars are evolved massive stars, undergoing extreme mass loss (10^{-5} to $10^{-4}\ M_\odot\,\mathrm{yr}^{-1}$), whose spectra show broad emission lines. Due to extensive mass loss, which has removed the outer hydrogen-rich layers of the star, the products of nuclear burning processes appear at the surface. WC stars are a particular class of WR stars whose spectra are dominated by emission lines of carbon, helium, and oxygen, and hence reflect material that has been partially processed by nuclear helium-burning. On the basis of the distribution of emission line strengths of different ionic species, WC stars are subdivided into spectral types from the "early" high-excitation type WC 4 to the "late" low-excitation type WC 9. The low metallicity (Z) in the LMC is expected to have significant consequences for the evolution of massive stars, mainly because O stars undergo lower mass loss for lower Z (Maeder 1991). According to standard evolutionary calculations the LMC WC stars arise from a smaller initial mass range and are expected to show higher carbon and oxygen surface abundances than their galactic counterparts. Observationally the galactic and LMC stellar populations differ in the ratio of WN to WC stars and the spectral subtype distribution. In the LMC one finds only early WC types (mainly WC 4), whereas late types (WC 7 - WC 9) are very common in the galaxy (Conti & Vacca 1990).

As a result of the known distance and the low internal reddening of the LMC, the HST provides the means to determine the absolute spectral energy distributions and hence reliable stellar luminosities, radii and mass loss rates. Through the possibility of a direct comparison of the model flux with the observation, difficulties concerning the continuum-definition are minimized. In combination with the high signal-to-noise ratio of the HST-data, reliable surface abundance determinations are possible.

The observations are presented in Sect. 2, followed by a brief description of the model calculations and the model atoms applied (Sect. 3). In Sect. 4 the analyses of the program stars including detailed comparisons between the observed and the synthetic spectra are presented. Finally we discuss the results with respect to their implications on massive stellar evolution (Sect. 5).

Table 1. Observed stars with names according to the catalogue of Breysacher (1981), and their alternate designations

Star	Alternate Designations
Br 7	HD 32125, WS 3, Sk -66°21, FD 4
Br 8	HD 32257, L-40, WS 4, Sk -69°42, FD 5
Br 10	HD 32402, AL-37, WS 6, Sk -68°15, BE-1717, FD 7
Br 43	HD 37026, S 41, AL-242, WS 31, Sk -67°144
Br 50	HD 37680, L-286, WS 35, Sk -69°191, BE-598
Br 74	HDE 269888, WS 42, Sk -69°234, BE-409, FD 61

2. Ultraviolet and optical spectra

The intention of the observational program is to obtain high quality spectrophotometric observations of a complete sample of "single" WC stars in the LMC. All stars with evidence for duplicity (i.e. those classified as WC+abs in the catalogue of Breysacher 1981) are excluded. Binary stars are excluded because we would need to allow for (the very uncertain) spectral contamination in the analysis, and because we wish to limit our discussion to single star evolution. The stars observed are summarized in Table 1 together with their alternate designations.

The ultraviolet spectra in the wavelength range from 1150-3300 Å are taken with the Faint Object Spectrograph (FOS) on board of Hubble Space Telescope (HST), between September '94 and June '95. The blue digicon and gratings G130H (1150-1606 Å), G190H (1573-2330 Å) and G270H (2222-3301 Å) are used in combination with the 0.26" round aperture (0.3), giving a resolution of about 0.9 Å for G130H, 1.4 Å for G190H and 1.9 Å for G270H, respectively. With total exposure times in the range from 22 min for the brightest star (Br 10) to 95 min for the faintest one (Br 74) a signal-to-noise ratio of about 30 is achieved.

For the optical range we use spectrophotometric data from the atlas by Torres & Massey (1987), covering the wavelength range from 3400-6800 Å with a resolution of 10-15 Å. For Br 10 we use our own optical spectrum with better resolution (about 3 Å) and higher S/N, which is taken at the ESO 3.6 m telescope in December 1989. With the ESO Faint Object Spectrograph (EFOSC), operated in the echelle spectroscopy mode using the Blue Cross Disperser (BCD), the wavelength range from 4000-7000 Å is covered. As our EFOSC spectrum is originally uncalibrated, it is scaled to the corresponding spectrum from Torres & Massey (1987).

3. Model atmospheres

The model calculations are very similar to those described in previous papers (Koesterke et al. 1992, Hamann et al. 1992, Koesterke & Hamann 1995, Leuenhagen & Hamann 1994, Leuenhagen et al. 1996). The standard model assumptions of spherically symmetric outflow, homogeneity and stationarity are adopted. Thus density and velocity stratifications are related by the equation of continuity.

Table 2. Summary of the model atoms

ion	grid models levels	line-fit models levels
He I	17	17
He II	16	16
He III	1	1
C II	3	3
C III	40	40
C IV	19	54
C V	1	1
O III	1	1
O IV	25	25
O V	36	36
O VI	15	15
O VII	1	1
total	175	210

The velocity field is prescribed by a stationary radial outflow with

$$v(r) = v_\infty \left(1 - \frac{R_0}{r}\right)^\beta . \quad (1)$$

This outer velocity law is augmented by an inner part which corresponds to an exponentially decreasing density distribution in the nearly hydrostatic domain. R_0 is suitably determined in order to connect both domains smoothly. The stellar core radius R_* is located at Rosseland optical depth of 20, the inner boundary of our model atmosphere. For all model calculations the exponent in the velocity law is set to $\beta = 1$.

The radiation transfer is calculated in the co-moving frame under non-LTE conditions, adopting a Doppler broadening velocity of $v_\mathrm{D} = 100\ \mathrm{km\,s^{-1}}$, and accounting for complex model atoms of helium, carbon and oxygen. Due to the large spherical extension of WR atmospheres, effective temperatures are related to a specified radius. The stellar temperature $T_\star$ is defined as the effective temperature related to $R_\star$. In this context each model atmosphere is specified by the stellar temperature $T_\star$, the stellar core radius $R_\star$, the terminal velocity v_∞, the mass loss rate $\dot{M}$, and the chemical composition, described by the carbon and oxygen mass fractions β_C and β_O. The number of free parameters is reduced by the introduction of the so-called transformed radius R_t, which can be considered to be a density parameter, connecting $R_\star$, $\dot{M}$ and v_∞ via the transformation law

$$R_\mathrm{t} = R_\star \left[\frac{v_\infty}{2500\,\mathrm{km\,s^{-1}}} \Big/ \frac{\dot{M}}{10^{-4}\,M_\odot\,\mathrm{yr^{-1}}} \right]^{2/3} . \quad (2)$$

For fixed R_t the model spectra (especially their line equivalent widths) are found to be nearly independent of the individual values of $R_\star$, $\dot{M}$ and v_∞ (Schmutz et al. 1989).

The radiation field is computed consistently with the equations of statistical and radiative equilibrium by the application of the ALI formalism (accelerated lambda iteration, cf. Hamann

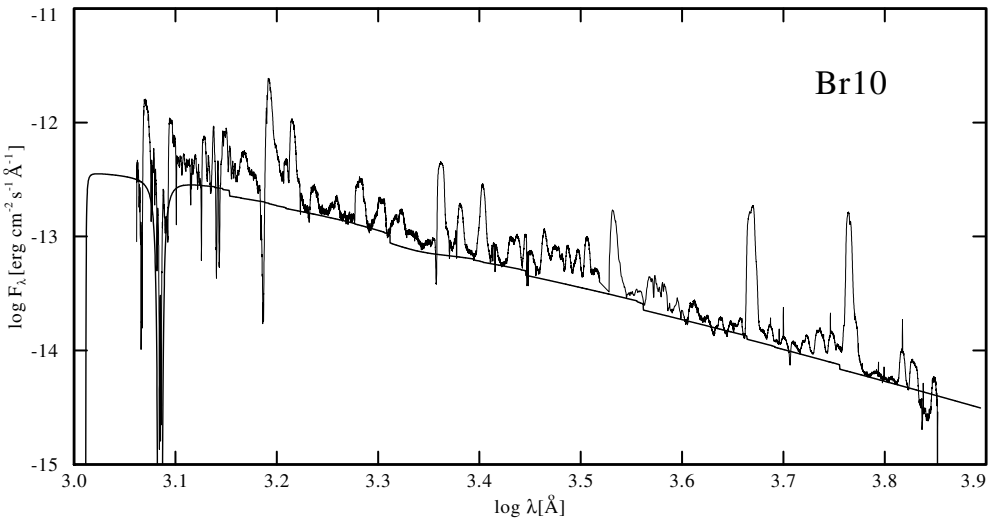

Fig. 1. Comparison of the model continuum flux (thick line) with the observed flux (thin line) of Br 10. A distance modulus of 18.5 is adopted. Reddening parameters according to Table 3 and Ly α absorption for a hydrogen column density of $7\,10^{21}$ cm^{-2} are applied to the model continuum

1985, 1986, 1987). The model atoms contain the relevant ionization stages (He I, He II, C II-C IV, O III-O VI). A summarizing description is given in Table 2.

After the determination of the population numbers and electron temperatures, the emergent flux is calculated for the whole observed spectral range by the solution of the Formal Integral in the observer's frame. The fine structure splitting is considered by assuming a relative LTE population for the angular momentum substates. Moreover the frequency redistribution of line photons by Thomson scattering is accounted for in the Formal Integral, as suggested by Hillier (1984, 1991) and adapted to our code by Hamann et al. (1992).

Line blanketing due to carbon and oxygen lines is included in our models, although metal line blanketing due to iron group elements is neglected. Pilot studies (Schmutz 1991, Hillier & Miller 1997) indicate that the expected impact on the analyses should be moderate. This is confirmed with preliminary calculations using the blanketed code of Hillier (Hillier & Miller 1997) which generally confirms the present analysis. While there is a suggestion from these models that the stellar luminosities may be slightly underestimated, and the O abundances overestimated in the present paper the differences are insufficient to affect any of our conclusions.

4. Analyses

The spectra of the six program stars are very similar, the differences in line equivalent widths amount to at most a factor of three. Prominent ionization species are He II, C III, C IV and O IV - O VI. To restrict the range of model parameters, a first comparison with a model grid with $T_\star$ = 60−180 kK, $\beta_{\rm C}$ = 0.25 and $\beta_{\rm O}$ = 0.15, covering a wide range in $R_{\rm t}$ is performed. Then a fine grid is calculated with an identical chemical composition, $T_\star$ = 60 − 130 kK and $R_{\rm t}$ restricted to a region where the observed ionization states and line strengths are reproduced. For the final quantitative analysis an extended model atom is used with all angular momentum states of the C IV ion up to n = 10 explicitly accounted for. This is necessary to avoid systematic errors concerning the determination of the carbon abundance (cf. Hamann 1992). The results of the analyses are listed in Table 3.

4.1. Continua

Due to the known distance to the LMC, its low reddening and the exact UV-photometry of HST, stellar luminosities can be determined with high accuracy through the comparison of model continua with observed fluxes. On this basis reliable stellar radii and mass loss rates can be determined. The observed fluxes are compared to reddened model continua, adopting a distance modulus of 18.5 mag (d = 50.1 kpc, cf. Jones et al. 1994). Galactic foreground reddening is accounted for according to Seaton (1979), with a standard color excess of $E^{\rm gal}_{B-V}$ = 0.03 mag. The contribution of the LMC is determined for each model calculation, by adjusting the extinction parameter to reproduce the slope of the observed continuum with the average extinction law of Howarth (1983). By this direct comparison of absolute fluxes, the problem of continuum normalization is reduced to the determination of the color excess.

The corresponding values for $E^{\rm LMC}_{B-V}$ are listed in Table 3. Only for Br 74, the faintest of the sample stars, is a value higher than 0.1 mag determined for the LMC contribution. After dereddening, the spectrum and luminosity of Br 74 turn out to be almost identical to that of Br 8. The strong similarity in the spectrum after dereddening suggests that the adopted interstellar LMC extinction law is valid, at least for Br 74 and Br 8. For the stars Br 7, Br 8, Br 43 and Br 50 Morris et al. (1993) obtained color excesses, assuming that the intrinsic continuum flux can be represented by a power law. For all these objects they determined low reddenings. Except for Br 7, for which they found $E^{\rm tot}_{B-V}$ = 0.01 ± 0.05, our values lie within the range of their 1σ error estimates.

As a result of our analyses we obtain stellar luminosities in the range from $10^{5.1}$ to $10^{5.6}\,L_\odot$. By the application of the stellar temperatures ($T_\star$) they translate into stellar radii ($R_\star$) from 1.1 to 2.5 $R_\odot$. The sensitivity of the derived luminosities

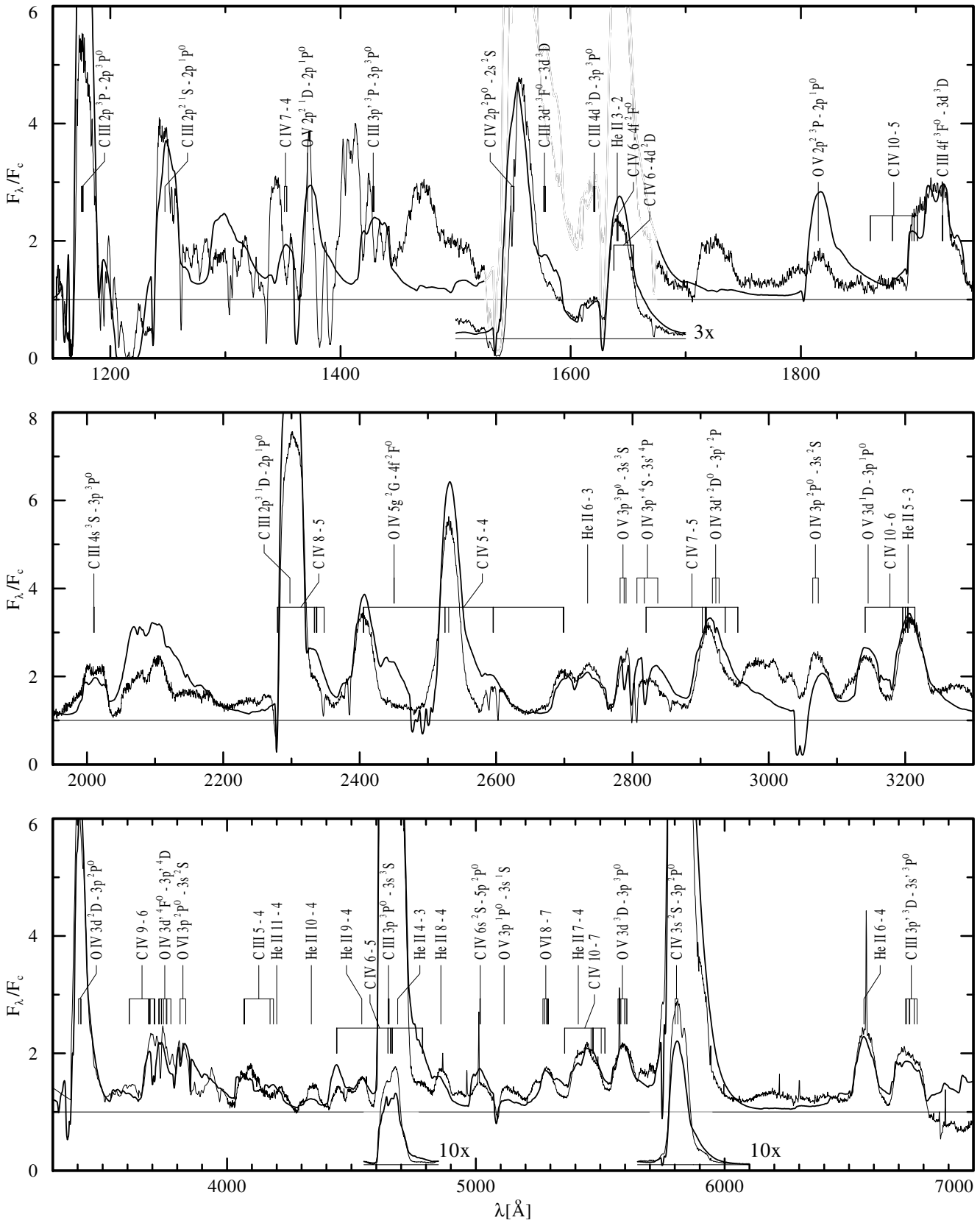

Fig. 2. Spectral fit for Br 10. The observation (thin line) is shown together with the synthetic spectrum (thick line). The model parameters are given in Table 3. The dominant line transitions are identified. The continuum is normalized by dividing the observed flux through the reddened model continuum. A correction for interstellar Ly α absorption with an adopted column density of 7 10^{21} cm^{-2} is applied to the model spectrum

Table 3. Results of the quantitative analyses: effective temperatures $T_\star$ and $T_{2/3}$, which refer to the radii $R_\star$ and $R_{2/3}$, respectively; transformed radius R_t according to Eq. (2); stellar core radius $R_\star$; radius $R_{2/3}$ where $\tau_\mathrm{Ross} = 2/3$; mass loss rate $\dot{M}$; terminal velocity v_∞; stellar luminosity L; surface mass fractions of carbon β_C and oxygen β_O; color excess due to internal LMC-reddening E_{B-V}^LMC; the numbers of ionizing photons emitted per second below the ionization edges of H I, He I and He II

Star	$T_\star$	$T_{2/3}$	R_t	$R_\star$	$R_{2/3}$	$\log \dot{M}$	v_∞	$\log L$	β_C	β_O	E_{B-V}^LMC	$\log(n_\mathrm{Phot}\ \mathrm{s}^{-1})$ below edge		
	[kK]	[kK]	$[R_\odot]$	$[R_\odot]$	$[R_\star]$	$[M_\odot\ \mathrm{yr}^{-1}]$	[km/s]	$[L_\odot]$	(mass fraction)		[mag]	H I	He I	He II
Br 7	94.6	49.8	2.00	1.65	3.60	-4.16	2300	5.29	0.4	0.2	0.08	49.17	48.88	38.23
Br 8	104.2	43.6	1.17	1.13	5.72	-4.06	2300	5.13	0.4	0.3	0.06	49.02	48.67	38.07
Br 10	92.5	45.6	2.00	2.52	4.11	-3.80	2800	5.62	0.5	0.2	0.05	49.50	49.20	38.64
Br 43	103.9	42.1	1.17	1.32	6.08	-3.91	2600	5.26	0.4	0.3	0.01	49.15	48.81	38.26
Br 50	94.0	38.8	1.58	2.25	5.86	-3.72	2800	5.55	0.4	0.1	0.05	49.43	49.11	38.31
Br 74	104.2	43.6	1.17	1.13	5.72	-4.06	2300	5.13	0.4	0.3	0.28	49.02	48.67	38.07

to a variation of the stellar temperature turns out to be relatively small. The effect of $T_\star$ on the bolometric correction is partly compensated by the necessary adjustment of the reddening correction. When models with similar line strengths are compared, the derived luminosities vary within ± 0.1 dex for the whole temperature range from $80 - 120$ kK. Variations of the wind density and the surface composition also affect the spectral energy distribution significantly. This becomes apparent in the fact that there exists no correlation between the visual magnitudes and luminosities derived for the sample stars.

The effect of line blanketing due to iron group elements on the spectral energy distribution is examined by test calculations with the code of Hillier (Hillier & Miller 1997). Models with similar spectral appearance and same visual brightness turn out to show higher fluxes in the wavelength range shortward of about 1100Å when line blanketing is accounted for. The effect on the derived numbers of emitted photons shortward of the edges of H I and He I (cf. Table 3) amounts to about 0.13 dex for the models under consideration.

The continuum fit for Br 10 is shown in Fig. 1. For $\log(\lambda) > 3.2$ the model agrees well with the observational data. At shorter wavelengths the pseudo-continuum of Fe V and Fe VI, which is not accounted for in these models, is clearly affecting the continuum energy distribution.

4.2. Spectral fits

The results of the quantitative analyses are listed in Table 3. Fig. 2 shows an example for the spectral fits. The observation is normalized by dividing the observed flux through the reddened model continuum, according to the results of the previous section.

Due to the inclusion of the UV spectral range, it is possible to determine the C III/C IV ionization structure very precisely by means of spectral lines like C III 1620, 1923, 2010 and 2297 Å and C IV 2405, 2525, 2595 and 2699 Å. The carbon mass fraction β_C can be derived to an accuracy of about 20% from the neighboring lines He II/C IV 5412/5470 Å and the UV-lines He II 2734 and 3204 Å. For the parameter range under consideration, the observed strengths of the helium and carbon lines can be reproduced for any temperature by choosing suitable values of R_t. Consequently a narrow strip in the $T_\star$-R_t-plane is defined by fitting these lines.

For a closer determination of the stellar parameters, oxygen lines have to be taken into account. The stellar temperature $T_\star$ and oxygen mass fraction β_O are adjusted by modeling the lines of the various oxygen ionization stages from O IV to O VI. Especially the lines of O V and O VI originate from relatively small spatial regions. Their strengths strongly depend on the detailed ionization structure and thus help to determine $T_\star$. O IV lines, on the other hand, are formed in the outer parts of the atmosphere, and depend mainly on the oxygen abundance. Unfortunately this dependence is relatively weak, and only O IV at 3070 Å is suitable for a quantitative analysis. Moreover, problems arise because too strong absorption components are predicted by our models for the O IV lines. Fig. 3 demonstrates the dependence of oxygen line strengths on oxygen abundance. Model spectra with β_O = 0.1, 0.2 and 0.3 are compared to the observation of Br 10. The oxygen abundance determination is accurate to $\pm 50\%$.

The determination of the terminal velocity (v_∞) is mainly based on the width of the prominent C III features, especially on the well defined absorption component of C III 2297 Å, because C III is dominant in the outer atmosphere and the ionization structure of carbon is well reproduced by our models. For the radial velocity of the LMC a standard value of 250 $\mathrm{km\,s^{-1}}$ (cf. Jones et al. 1994) has been adopted. The accuracy for the determination of v_∞ amounts to about ± 150 $\mathrm{km\,s^{-1}}$.

The C IV 1550 Å resonance doublet, which is commonly used for the determination of terminal velocities, is not well reproduced by our calculations. In addition to the massive interstellar contamination, which causes a depression of the blue wing of this line, redistribution and line broadening effects which possibly are of great importance for the formation of resonance lines, are not included into our code.

Carbon-to-helium ratios of three of the sample stars (Br 7, Br 8 and Br 74) have been determined previously by Torres (1988) by means of optical and infrared recombination line analysis. Because the ionization structure of the atmosphere was not accounted for in her work, her results are only approximate. The carbon ratios obtained in the present work are about a factor of two higher.

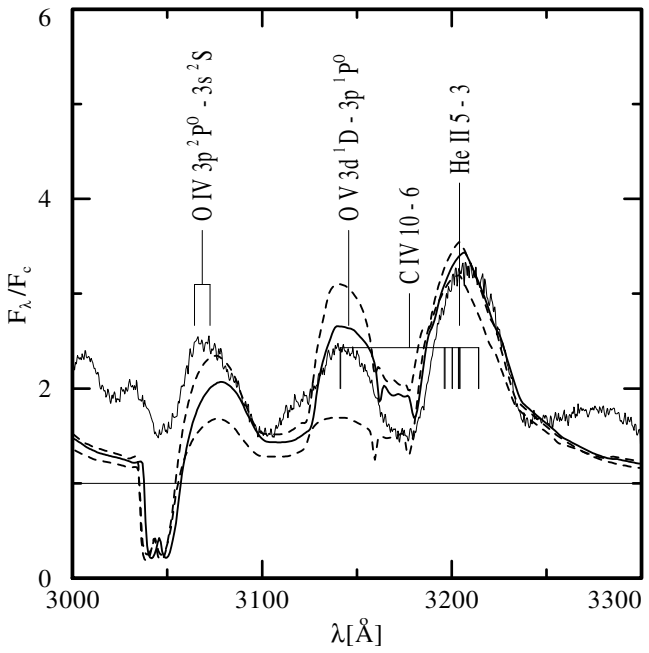

Fig. 3. Synthetic spectra with a carbon mass fraction of $\beta_C = 0.5$ and different oxygen mass fractions are compared to the observation of Br 10 (thin line): $\beta_O = 0.2$ (thick line) and $\beta_O = 0.1$ and 0.3 (dashed lines)

Terminal velocities have been derived by Torres et al. (1986) for all program stars, by extrapolating the line widths of recombination lines of the visible ionic species to zero ionization potential. They measured velocities appreciably higher than the ones we obtained. These discrepancies may be explained by the severe line blending in WC stars, and by the difficulties of converting the FWHM velocities Torres et al. measured to a terminal velocity. Our terminal velocities are confirmed by the spectral synthesis, which shows that the line widths are in good agreement over the entire observed spectral range.

4.3. Differences among the program stars

Although the luminosities of the program stars cover a range from $10^{5.1} - 10^{5.6}\,L_\odot$, their spectra appear very similar. The slight differences among them translate into just as slight differences in the model parameters. The main constraint on the possible parameter range is provided by the complex ionization structure of oxygen. As a result, models with fixed luminosity are restricted to a defined density structure in the optically thin parts of the atmosphere, which slightly changes with stellar temperature. To reproduce the small differences in the C III/C IV line strengths, a small variation of the density is necessary, which is compensated by a variation of $T_\star$.

The surface abundances mainly differ in the oxygen-to-helium ratio. As mentioned previously, the accuracy of the oxygen abundance determination is low, but the relative differences should be reproduced correctly.

Table 4. Radiative luminosities $L_\star$ and nuclear luminosities $L_{\rm nuc}$ which include the additional flux of wind energy according to Heger & Langer (1996). Theoretical values for the stellar masses $M_\star^{\rm th}$ and radii $R_\star^{\rm th}$ are derived from $L_{\rm nuc}$ according to Langer (1989a). The spectroscopically derived radii $R_\star^{\rm spec}$ are in general agreement with the theoretical values. The importance of wind darkening for the derivation of theoretical radii and masses is demonstrated by giving the uncorrected values for the radii ($R'_\star$) and masses ($M'_\star$) determined from $L_\star$ only

Star	$\log L_\star$ $[L_\odot]$	$\log L_{\rm nuc}$ $[L_\odot]$	$R_\star^{\rm spec}$ $[R_\odot]$	$R_\star^{\rm th}$ $[R_\odot]$	$R'_\star$ $[R_\odot]$	$M_\star^{\rm th}$ $[M_\odot]$	$M'_\star$ $[M_\odot]$
Br 7	5.29	5.43	1.65	1.22	1.09	13.4	11.2
Br 8	5.13	5.35	1.13	1.10	0.94	11.8	9.1
Br 10	5.62	5.79	2.52	1.78	1.48	21.8	17.1
Br 43	5.26	5.52	1.32	1.35	1.07	14.8	10.6
Br 50	5.55	5.78	2.25	1.71	1.34	21.9	15.9
Br 74	5.13	5.35	1.13	1.10	0.94	11.8	9.1

5. Discussion

5.1. Evolutionary status

WC stars represent late evolutionary stages of massive stars. Due to extensive mass loss in their evolutionary history, layers which have undergone helium burning are exposed at the stellar surface. Such stars are composed of a large helium-burning convective core and a relatively small radiative envelope. They are expected to be nearly chemically homogeneous, because the time scale for stripping off the envelope mass is shorter than the corresponding helium burning time scale. According to Langer (1989a) the basic parameters characterizing a WC star are its mass and chemical surface composition. In a further study Heger & Langer (1996) found that the influence of the stellar wind on the subsonic layers is negligible and that the radius of hydrostatic stellar models coincides with the sonic point in hydrodynamic calculations. Due to this fact the spectroscopically determined stellar core radii ($R_\star$) can be compared to theoretical surface radii.

For the examination of the consistency of our results with stellar structure calculations we perform a comparison of the spectroscopically derived radii and luminosities with the mass-luminosity and mass-radius relations from Langer (1989a). A comparison with computed HRD-positions remains ambiguous, because of the unknown relation between stellar parameters and wind structure. Due to the large spherical extension of the atmospheres the effective temperature depends on the definition of a stellar surface radius.

Problems also arise with the definition of the stellar luminosity, because the observed mass loss contributes significantly to the total amount of energy emitted by the star. Therefore the radiative luminosity $L_\star$ which is determined in our spectral analyses is significantly lower than the total luminosity produced by nuclear burning processes ($L_{\rm nuc}$), which is the quantity that has to be considered for comparisons with stellar structure calculations. The main part of this "wind darkening" is caused by the mechanical and gravitational energy needed to lift the matter away from the stellar surface to the high observed velocities.

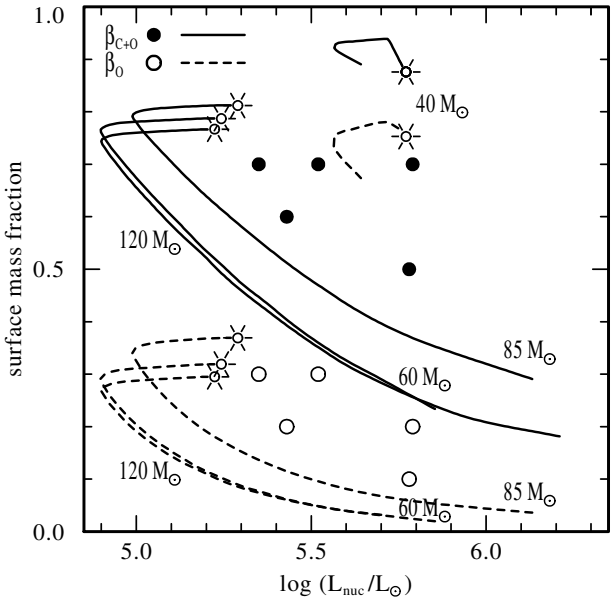

Fig. 4. Plot of observed surface abundances $\beta_{\rm O}$ (○) and $\beta_{\rm C+O}$ (●) vs. nuclear luminosities, compared to $\beta_{\rm O}$ (dashed line) and $\beta_{\rm C+O}$ (solid line) according to evolutionary calculations with high mass loss rates from Meynet et al. (1994) for Z = 0.008. The nuclear luminosities are corrected for the contribution of the stellar wind to the total luminosity. Stellar tracks for the whole initial mass range with considerable amounts of carbon at the surface are shown. The end of the evolutionary sequences is indicated by supernova symbols

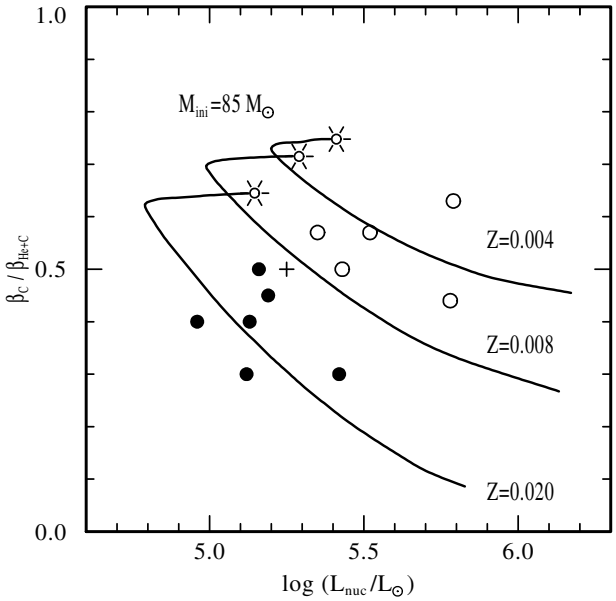

Fig. 5. Plot of observed carbon surface mass fractions related to carbon and helium vs. nuclear luminosities. WC stars with known distance in the LMC (○) and the galaxy (● strong-lined, + weak-lined) are compared to evolutionary calculations with high mass loss from Meynet et al. (1994). Evolutionary tracks with an initial mass of 85 $M_\odot$ are plotted for different metallicities. The observed values for the galactic sample are taken from Koesterke & Hamann (1995). The luminosities are corrected for the contribution of the stellar wind to the total luminosity

Heger & Langer (1996) calculated a further correction for the energy and the change of enthalpy of the material which is lifted from inside the star to the sonic radius. In Table 4 the spectroscopically determined luminosities ($L_\star$) are listed together with the nuclear luminosities ($L_{\rm nuc}$) which have been corrected for these effects. The theoretical radii and masses used for this correction are taken from Langer (1989a). Due to the higher nuclear luminosities, higher stellar masses and radii are derived. To demonstrate this effect, theoretical radii and masses obtained from the uncorrected stellar luminosities ($L_\star$) are also listed.

When the empirically determined stellar core radii $R_\star$ are compared to the theoretical values $R_\star^{\rm th}$, the agreement is better than 5% for three of the program stars (cf. Table 4). For the rest of the stars the stellar radii derived in the present work are less than a factor 1.4 higher than theoretically predicted. This is no contradiction to theory, because due to the large optical depths in the continuum, spectral information is only obtained from layers far above the hydrostatic radius. The actual density distribution in the deep layers near the hydrostatic radius may differ from that given by the standard β-velocity law we have adopted for our model calculations.

The stellar evolution in the WC phase depends on the duration of central He-burning in combination with the change of stellar mass due to mass loss. For the present work the effects of the low metallicity in the LMC are of special concern. In low metallicity environments, lower mass loss rates are expected for the O star phase. In effect the WR phase is reached later. In this case the convective-core mass is larger during the WN phase, and the lower mass limit for stars reaching the WC phase is higher. Thus higher WC masses and luminosities are expected. Due to the longer duration of helium burning in pre-WC stages, higher carbon and oxygen fractions are reached when the WC phase is entered (Meynet et al. 1994).

In He-burning stars the carbon-to-oxygen ratio is adjusted by two reactions. At the beginning of the He-burning phase the dominant reaction is $3\,\alpha \rightarrow {}^{12}$C. It is gradually taken over by ${}^{12}{\rm C} + \alpha \rightarrow {}^{16}{\rm O}$ with increasing ^{12}C-abundance. In effect the carbon abundance increases until the conversion from carbon to oxygen dominates. Because the central temperature is nearly independent of the stellar mass, the maximum carbon abundance depends essentially on the ratio of the $3\,\alpha$ reaction rate to that from ^{12}C to ^{16}O. The maximum carbon mass fraction encountered empirically thus sets an upper limit to the latter of the two rates, which is still uncertain.

We detected nearly the same carbon abundances ($\beta_{\rm C} \simeq 0.4$) for all of the sample stars. With respect to the accuracy of our abundance determinations, a value lower than 0.3 can be excluded for all of the observed stars. For Br 10 a value of $\beta_{\rm C} = 0.4 - 0.6$ is found. Hence a lower limit of about 0.4 is set for the maximum carbon mass fraction by this observation. This value is in agreement with the maximum value reached in evolutionary calculations for massive stars, like Schaller et al.

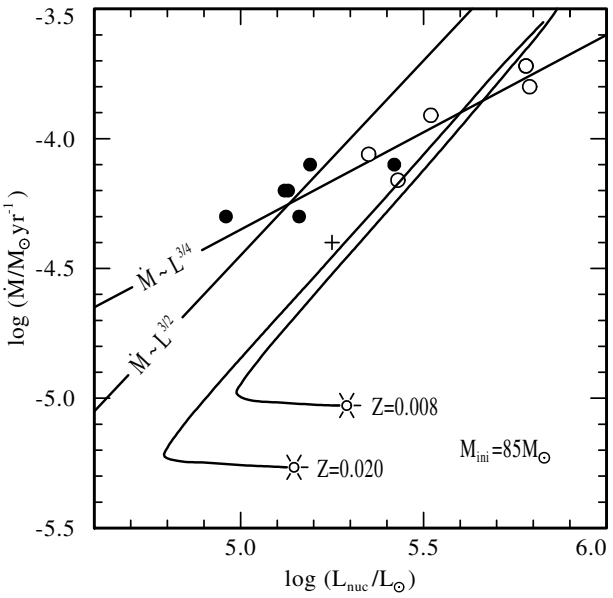

Fig. 6. Plot of observed mass loss rates vs. nuclear luminosities for WC stars with known distance in the LMC (○, this work) and the galaxy (● strong-lined, + weak-lined, Koesterke & Hamann 1995). A comparison to the tentative fit for galactic hydrogen-free stars with $\log[\dot{M}/(M_\odot\,\mathrm{yr}^{-1})] = 1.5\log(L/L_\odot) - 11.95$ according to Hamann (1995), and to the mass loss rates adopted by Meynet et al. (1994) for WC stars with initial masses of 85 $M_\odot$ is performed. The strong-lined WC stars of both samples obey a relation of the form $\log[\dot{M}/(M_\odot\,\mathrm{yr}^{-1})] = 0.75\log(L/L_\odot) - 8.5$

(1992), who took the $^{12}\mathrm{C}\,(\alpha,\gamma)\,^{16}\mathrm{O}$ reaction rate from Caughlan et al. (1985).

In Fig. 4 the observed surface mass fractions are plotted versus the corresponding nuclear luminosities. They are compared to evolutionary tracks from Meynet et al. (1994) for $Z = 0.008$ in the relevant initial mass range. Meynet et al. adopted mass loss rates enhanced by a factor of two for the O and WNL phases with respect to the grid of Schaerer et al. (1993). With the exception of the prescriptions for the mass loss rates, Meynet et al. used the same physical ingredients as Schaerer et al. The observed range of WC luminosities and surface compositions, and the gradual increase of the oxygen abundance with decreasing luminosity is in agreement with the calculations of Meynet et al. With standard mass loss rates Schaerer et al. obtain luminosities greater than $10^{5.6} L_\odot$ and oxygen surface mass fractions higher than 0.5 for all WC phases, in contradiction to the observed values. Enhanced mixing also lowers the C/He and O/He abundance ratios (Maeder 1987), and provides an alternate mechanism to the use of enhanced mass loss rates to explain our observed abundance ratios.

5.2. Comparison to galactic WC stars

In Fig. 5 the luminosities and carbon abundances of the LMC stars are compared to galactic WC stars with known distances according to NLTE-analyses from Koesterke & Hamann (1995). Because the latter did only include helium and carbon, the ratio $\beta_\mathrm{C}/\beta_\mathrm{C+He}$ has to be considered for a comparison. All luminosities are corrected for the contribution of the stellar wind to the total luminosity. Evolutionary tracks with an initial mass of 85 $M_\odot$ are plotted for different metallicities. The two samples differ in the expected way: the LMC stars are more luminous and their surface carbon fractions are higher.

5.3. Mass loss rates

The observed mass loss rates are of special interest because of their strong influence on the stellar evolution in the WC phase. In Fig. 6 the results of our analyses are presented together with mass loss rates of galactic WC stars with known distances from Koesterke & Hamann (1995). For comparison we also show the values used by Meynet et al. (1994) for their evolutionary calculations (displayed are tracks for initial mass of 85 $M_\odot$ and two different metallicities), who adopted Langer's (1989b) suggestion of a mass-dependent mass loss rate. The straight line with slope 3/2 was proposed by Hamann (1995) for galactic hydrogen-free WN stars. With our correction for the wind luminosity, the galactic WC sample now coincides with that relation. The straight line with slope 3/4 gives a tentative fit to the whole sample of galactic and LMC stars. However, the LMC and the galactic WC stars build up two disjoint groups of luminosities, and therefore it cannot be decided whether these stars follow a common $\dot{M}$-L-relation, or if the LMC stars have lower mass loss rates due to their lower metallicity.

The study of early WC stars in high metallicity environments like M 31 would help to settle these questions. Furthermore the direct determination of Fe and Si abundances is now possible.

One concern with the mass-loss rates is the possibility that they have been overestimated due to inhomogeneities in the stellar wind. Simplistic calculations using the code of Hillier and a filling factor approach (Hillier 1996) show that the spectra of the LMC WC stars can be reproduced with mass-loss rates a factor of 3 lower. Quantitatively the fits obtained are virtually indistinguishable from those without clumping. The broadening on the red side of the profiles in the clumped models is probably in better agreement with observations, but a strong verification of this statement is difficult because of the extreme blending in WC spectra. As noted by our earlier discussion a factor of 3 reduction in mass-loss rate would have a profound influence on the evolutionary models.

6. Conclusion

By the inclusion of oxygen into our NLTE models, it is possible to reproduce the observed spectra of WC stars of early spectral subtype. For a sample of LMC-WC stars, basic stellar parameters are derived: surface mass fractions, stellar luminosities, mass loss rates, terminal wind velocities and effective temperatures related to a specified radius. The flux of wind energy is found to contribute significantly to the total luminosities. The chemical compositions and nuclear luminosities are in general agreement with the evolutionary calculations for $Z = 0.008$ of

Meynet et al. (1994), who adopted high mass loss rates for the O and WNL phases. Luminosities and carbon surface abundances are found to be higher than for galactic WC stars. The observed mass loss rates in the LMC are in agreement with standard relations. Related to their lower luminosities, galactic WC stars show a tendency towards higher mass loss rates. This may reflect a metallicity effect or a flat slope of the relation between stellar luminosity and mass loss for WC stars.

Acknowledgements. This work was supported by the Deutsche Agentur für Raumfahrtangelegenheiten under grant DARA 50 OR 9605 7. Hillier acknowledges support by NASA through grant numbers 4450.01-92A and 5460.01-93A from the STScI, which is operated by AURA, under NASA contract NAS5-26555. The calculations were performed on the CRAY computers of the Rechenzentrum der Universität Kiel and the Konrad-Zuse-Zentrum für Informationstechnik Berlin. The HST observations were obtained with U. Wessolowski, K. Butler, R.P. Kudritzki, D.J. Lennon and S.A. Voels as Co-Investigators. We thank D. Miller for preparing the HST spectra, and for his contribution to the piloting line-blanketed models. We acknowledge very useful discussions with N. Langer.

References

Breysacher J. 1981, A&AS 43, 203
Caughlan G.R., Fowler W.A., Harris M.J., Zimmermann B.A. 1985, Atomic Data Nuc. Data Tables 32, 197
Conti P.S., Vacca D. 1990, AJ 100, 431
Hamann W.-R. 1985, A&A 148, 364
Hamann W.-R. 1986, A&A 160, 347
Hamann W.-R. 1987, in "Numerical Radiative Transfer", ed. W. Kalkofen, Cambridge University Press, p. 35
Hamann W.-R. 1995, in "Wolf-Rayet Stars: Binaries, Colliding Winds, Evolution", K.A. van der Hucht and P.M. Williams (eds.), IAU Symp. No. 163, Kluwer, Dordrecht, Holland, p105
Hamann W.-R. 1996, in "Hydrogen-Deficient Stars", C.S. Jeffery and U. Heber (eds.), ASP Conf. Series, Vol. 96, p. 127
Hamann W.-R., Koesterke L. 1993, in "Planetary Nebulae", R. Weinberger and A. Acker (eds.), Proc. IAU Symp. No. 155, p. 87
Hamann W.-R., Leuenhagen U., Koesterke L., Wessolowski U. 1992, A&A 255, 200
Heger A., Langer N. 1996, A&A 315, 421
Hillier, D.J. 1984, ApJ, 280, 744
Hillier D.J. 1989, ApJ 347, 392
Hillier D.J. 1991, A&A 247, 455
Hillier D.J. 1996, in "Wolf-Rayet Stars in the Framework of Stellar Evolution", J.M. Vreux, A. Detal, D. Fraipont-Caro, E. Gosset, G. Rauw (eds.), Proc. of the 33rd Liège International Astrophysical Colloquium, p. 509
Hillier D.J., Miller D.L. 1997, ApJ submitted
Howarth I.D. 1983, MNRAS 203, 301
Jones B.F., Klemola A.R., Lin D.N.C. 1994, AJ 107, 1333
Koesterke L., Hamann W.-R., Wessolowski U. 1992, A&A 261, 535
Koesterke L., Hamann W.-R. 1995, A&A 299, 503
Langer N. 1989a, A&A 210, 93
Langer N. 1989b, A&A 220, 135
Leuenhagen U., Hamann W.-R. 1994, A&A 283, 567
Leuenhagen U., Hamann W.-R., Jeffery C.S. 1996, A&A (in press)
Maeder A. 1987, A&A, 173, 246
Maeder A. 1991, in "Wolf-Rayet Stars and Interrelations with other Massive Stars in Galaxies", K. A. van der Hucht and B. Hydayat (eds), IAU Symp. No. 143, Kluwer, Dordrecht, Holland, p575
Meynet G., Maeder A., Schaller G., Schaerer D., Charbonnel C. 1994, A&AS 103, 97
Morris P.W., Brownsberger K.R., Conti P.S., Massey P., Vacca W.D., 1993, ApJ 412, 324
Schaerer D., Meynet M., Maeder A., Schaller G. 1993, A&AS 98, 523
Schaller G., Schaerer D., Meynet G., Maeder A. 1992, A&AS 96, 269
Schmutz W., Hamann W.-R., Wessolowski U. 1989, A&A 210, 236
Seaton M.J. 1979, MNRAS 187, 73P
Torres A.V., Conti P.S., Massey P. 1986, ApJ 300, 379
Torres A.V., Massey P. 1987, ApJ Suppl. 65, 459
Torres A.V. 1988, ApJ 325, 759

This article was processed by the author using Springer-Verlag LaTeX A&A style file *L-AA* version 3.